DOI: 10.1002/cphc.200700003

Parameterization of Peptide ^{13}C Carbonyl Chemical Shielding Anisotropy in Molecular Dynamics Simulations**

Daniel M. Jordan,[a, d] K. Maria Mills,[b] Ioan Andricioaei,[b] Akash Bhattacharya,[a] Kim Palmo,*[a, c] and Erik R. P. Zuiderweg*[a]

NMR chemical shielding anisotropy (CSA) relaxation is an important tool in the study of dynamical processes in proteins and nucleic acids in solution. Herein, we investigate how dynamical variations in local geometry affect the chemical shielding anisotropy relaxation of the carbonyl carbon nucleus, using the following protocol: 1) Using density functional theory, the carbonyl $^{13}C'$ CSA is computed for 103 conformations of the model peptide group N*-methylacetamide (NMA). 2) The variations in computed $^{13}C'$ CSA parameters are fitted against quadratic hypersurfaces containing cross terms between the variables. 3) The predictive quality of the CSA hypersurfaces is validated by comparing the predicted and de novo calculated $^{13}C'$ CSAs for 20 molecular dynamics snapshots. 4) The CSA fluctuations and their autocorrelation and cross correlation functions due to bond-length and bond-angle distortions are predicted for a chemistry Harvard molecular mechanics (CHARMM) molecular dynamics trajectory of Ca^{2+}-saturated calmodulin and GB3 from the hypersurfaces, as well as for a molecular dynamics (MD) simulation of an NMA trimer using a quantum mechanically correct forcefield. We find that the fluctuations can be represented by a 0.93 scaling factor of the CSA tensor for both R_1 and R_2 relaxations for residues in helix, coil, and sheet alike. This result is important, as it establishes that $^{13}C'$ relaxation is a valid tool for measurement of interesting dynamical events in proteins.*

Introduction

NMR chemical shielding anisotropy (CSA) relaxation is an important tool in the study of dynamical processes in proteins and nucleic acids in solution.[1–4] The $^{13}C'$ CSA relaxation of proteins in particular is increasingly used, in addition to NH dipolar relaxation, to help characterize the dynamical processes of the protein backbone.[5–11] However, it was realized that the $^{13}C'$ CSA is not constant for the different amino acids in a protein.[5,9–13] In particular, the central component σ_{yy} and the angle of the σ_{zz} principal axis can vary by 20 ppm and 20°, respectively, over the protein sequence.[9,10] This has lead to the development of $^{13}C'$ relaxation fitting programs that take these variations into account as a fitted parameter.[10,14]

Herein, we investigate the origins of the variation of the $^{13}C'$ CSA tensor in depth. By using DFT calculations, we find that the principal values and orientations of the tensor are very sensitive to small local changes in structure, such as changes in bond lengths and bond angles involving the C′ atom. This observation immediately suggests that the CSA will fluctuate as a function of time when bond lengths and angles fluctuate, as is to be expected in peptides and proteins in the aqueous phase. This effect raises several questions: 1) How large can the fluctuations of the principal values and orientations of the CSA be? 2) What is the correlation time of these fluctuations? 3) Are these fluctuations relaxation active, or can one capture the time variation as a dynamic average, which scales the CSA? 4) How do these variations affect $^{13}C'$ relaxation rate determinations?

Most of the questions raised could be answered if the $^{13}C'$ CSA could be accurately computed for snapshots of reliable molecular dynamics (MD) calculations. However, this approach is not (yet) feasible. Even for the smallest of molecular fragments representing a protein, for example, the 12-atom molecule *N*-methylacetamide (NMA), adequate-level DFT calculations of the CSAs will take about an hour on a modern workstation. Hence, to characterize CSA fluctuations in an actual molecular dynamics run of even such a tiny molecule will take years of computational time. Certainly, dynamical CSA calculations on full proteins cannot even be contemplated to date.

[a] *D. M. Jordan, A. Bhattacharya, Dr. K. Palmo, Prof. Dr. E. R. P. Zuiderweg*
Biophysics Research Division and
Departments of Biological Chemistry and Chemistry
University of Michigan, 930 N. University Ave
Ann Arbor, Michigan 48109 (USA)
Fax: (+1) 734-7643323
E-mail: Zuiderwe@umich.edu

[b] *K. M. Mills, Prof. Dr. I. Andricioaei*
Department of Chemistry and
The Center for Computational Medicine and Biology and
Program in Biophysics
University of Michigan, Ann Arbor, MI (USA)

[c] *Dr. K. Palmo*
D. E. Shaw Research, LLC, New York, NY 10036 (USA)

[d] *D. M. Jordan*
Department of Physics, Yale University, New Haven, CT (USA)

[**] *Effects of Dynamic Local Distortions on ^{13}C Carbonyl NMR Relaxation.*

Herein, we explore whether it is possible to reliably parameterize the $^{13}C'$ CSA in NMA as a function of simple molecular parameters such as bond lengths, bond angles, and hydrogen bonding. If so, it would provide a way to predict the CSA of snapshots of a molecular dynamics simulation in a very efficient way.

Results and Discussion

Parameter Fitting

Bond Lengths and Angles

The reference NMA model (Figure 1) was optimized by DFT computations as afforded by the Gaussian 03 software package at the B3PW91/6-31G level. Test CSA calculations and geometry optimizations on the reference were also carried out with the higher-level 6-31+G** and 6-31++G** basis sets. The differences between these calculations and those performed with the 6-31G basis set were in each case less than 5 ppm. Hence, it was concluded that the 6-31G basis set was sufficient for the CSA calculations.

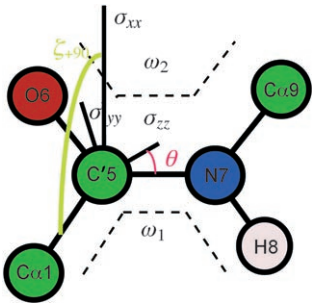

Figure 1. Cartoon of the peptide plane in the NMA molecule, which serves to define the atomic and molecular parameters used to characterize the $^{13}C'$ CSA, as well as the $^{13}C'$ CSA components themselves. The atom numbering is shown.

The parameterization calculations were done by perturbing the internal coordinates of the reference model. For each of the relevant variables, five values were considered, as shown in Table 1. For bond lengths, these were $\delta_{eq}\pm0.02$ Å and $\delta_{eq}\pm0.01$ Å in addition to the equilibrium distance in the reference structure (δ_{eq}). For bond angles, we used $\phi_{eq}\pm10^\circ$, $\phi_{eq}\pm5^\circ$ in addition to the equilibrium angle ϕ_{eq}. For dihedrals, we used $\omega_{eq}\pm30$, $\omega_{eq}\pm15^\circ$ in addition to equilibrium dihedral ω_{eq}.

Many of the perturbations are coupled group-wise with respect to the CSA computation. Hence, the CSA hypersurfaces were explored for the NMA model by constructing 65 conformations around the C′ atom (parameters 1–5), 33 conformations around the N atom (parameters 7–10), and 5 d_{NH} distances, for a total of 103 independent conformations. Each of the conformations was minimized while keeping the perturbations fixed. Second-order effects of this minimization, such as changes in N parameters caused by minimizing a structure with fixed but perturbed C parameters did occur, but these changes had negligible effects on the computed $^{13}C'$ CSA values.

The hypersurfaces for the CSA values were fitted using the program Mathematica 5.2. It was determined that a fit using a quadratic approximation for each dimension and each cross term was sufficiently accurate; using cubic approximations or including cross terms between more than two of the basis vectors did not improve the fit.

For the CSA orientation hypersurface, several functionalities were surveyed. The best was to fit cosθ, where θ is the angle between the CSA σ_{zz} axis and the C′–N bond vector, against a quadratic equation in the parameters. The angle ζ, which describes the angle between the normal of the peptide plane and the CSA σ_{xx} axis, was best parameterized as a sine function.

The resulting parametric equations are listed in Table 2. A sample two-dimensional cross section through the hypersurfaces is shown in Figure 2.

Hydrogen Bonding

It has been documented that the $^{13}C'$ CSA varies as function of hydrogen bonding of the carbonyl oxygen atom.[15] Following a similar protocol as for the bond lengths, parameterization calculations were carried out at the B3PW91/6-31G level while restraining either the O–N H-bond distance between two adjacent NMA molecules or the O–H–N H-bond angle. The parameterization is listed in Table 3. A graph showing the data points and the fitting (Figure 3) indicates that variation in hydrogen bonding does not affect the $^{13}C'$ nearly as much as the variations in local geometry.

Table 1. Ranges of parameter variation.

Parameter	Variable	Equilibrium value	Range	Effect on CSA	Covariance
1	$\delta_{C'O}$	1.2497	±0.02 Å	±5.6 ppm	1–5
2	$\delta_{C'C\alpha1}$	1.5121	±0.02 Å	±2.3 ppm	1–5
3	$\delta_{C'N}$	1.3693	±0.02 Å	±0.9 ppm	1–5
4	$\phi_{C\alpha1C'N}$	115.6745	±5°	±3 ppm	1–5
5	$\phi_{C\alpha1C'O}$	121.7513	±5°	±1 ppm	1–5
6	δ_{NH}	1.0075	±0.02 Å	±0.5 ppm	6
7	$\phi_{C'NH}$	119.0901	±5°	±0.7 ppm	7–10
8	$\phi_{C'NC\alpha2}$	122.1158	±5°	±1.1	7–10
9	ω_1 (Cα1C′NH)	0.0846	±10°	±0.5	7–10
10	ω_2 (OC′NCα2)	−0.1103	±10°	±0.5	7–10

Validation

The parameterization of the $^{13}C'$ CSA was validated with 20 arbitrarily chosen conformations for the NMA molecule. The conformations were taken from a spectroscopically determined force field (SDFF) molecular dynamics trajectory of an NMA trimer at 40 K (see the Experimental Section). For each of the 20 structures, the $^{13}C'$ CSA and

Table 2. Empirical parametric equations describing the $^{13}C'$ CSA dependence on local geometry parameters in NMA.[a]

$$\sigma_{zz} = -52.73 + 0.089\,\phi_{C\alpha-C'-O} - 0.005242\,\phi^2_{C\alpha-C'-O} - 0.4789\,\phi_{C\alpha-C'-N} - 0.02368\,\phi_{C\alpha-C'-O}\phi_{C\alpha-C'-N} - 0.005242\,\phi^2_{C\alpha-C'-N} - 7.999\delta_{C\alpha-C'} - 0.5800\,\phi_{C\alpha-C'-O}\delta_{C\alpha-C'} + 0.2172\,\phi_{C\alpha-C'-N}\delta_{C\alpha-C'} - 327.6\delta^2_{C\alpha-C'} - 384.0\delta_{C'-O} + 0.5073\,\phi_{C\alpha-C'-O}\delta_{C'-O} - 1.819\,\phi_{C\alpha-C'-N}\delta_{C'-O} - 7.636\delta_{C\alpha-C'}\delta_{C'-O} - 327.7\delta^2_{C'-O} - 28.91\delta_{C'-N} - 0.1631\,\phi_{C\alpha-C'-O}\delta_{C'-N} + 22.54\,\phi_{C\alpha-C'-N}\delta_{C'-N} + 2.048\delta_{C\alpha-C'}\delta_{C'-N} - 19.77\delta_{C'-O}\delta_{C'-N} - 327.6\delta^2_{C'-N} + 0.7418\,\phi_{C'-N-H} + 0.001702\,\phi^2_{C'-N-H} - 0.2911\,\phi_{C'-N-} - 0.004877\,\phi_{C'-N-H}\phi_{C'-N-C\alpha} + 0.001700\,\phi^2_{C'-N-C\alpha} + 0.001400\omega_1 + 0.00002690\,\phi_{C'-N-H}\omega_1 - 0.00002336\,\phi_{C'-N-C\alpha}\omega_1 - 0.009691\omega^2_1 - 0.001331\omega_2 - 0.00001943\,\phi_{C'-N-H}\omega_2 + 0.00002123\,\phi_{C'-N-C\alpha}\omega_2 + 0.01459\omega_1\omega_2 - 0.009691\omega^2_2 + 5.931\delta_{H-N} - 381.8\delta^2_{H-N}$$

$$\sigma_{yy} = 45.92 + 0.1215\,\phi_{C\alpha-C'-O} - 0.006612\,\phi^2_{C\alpha-C'-O} - 0.09402\,\phi_{C\alpha-C'-N} - 0.01278\,\phi_{C\alpha-C'-O}\phi_{C\alpha-C'-N} - 0.006612\,\phi^2_{C\alpha-C'-N} + 48.50\delta_{C\alpha-C'} - 0.6417\,\phi_{C\alpha-C'-O}\delta_{C\alpha-C'} - 0.3423\,\phi_{C\alpha-C'-N}\delta_{C\alpha-C'} - 413.3\delta^2_{C\alpha-C'} - 223.4\delta_{C'-O} + 1.048\,\phi_{C\alpha-C'-O}\delta_{C'-O} + 0.872\,\phi_{C\alpha-C'-N}\delta_{C'-O} - 116.8\delta_{C\alpha-C'}\delta_{C'-O} 413.3\delta^2_{C'-O} - 14.18\delta_{C'-N} - 0.2070\,\phi_{C\alpha-C'-O}\delta_{C'-N} + 11.85\,\phi_{C\alpha-C'-N}\delta_{C'-N} - 17.87\delta_{C\alpha-C'}\delta_{C'-N} + 5.29\delta_{C'-O}\delta_{C'-N} - 413.3\delta^2_{C'-N} + 0.2876\,\phi_{C'-N-H} + 0.06843\,\phi^2_{C'-N-H} + 1.743\,\phi_{C'-N-C\alpha} - 0.03273\,\phi_{C'-N-H}\phi_{C'-N-C\alpha} + 0.06843\,\phi^2_{C'-N-C\alpha} + 0.001650\omega_1 - 0.00002733\,\phi_{C'-N-C\alpha}\omega_1 - 0.008761\omega^2_1 - 0.001682\omega_2 + 0.00003240\,\phi_{C'-N-C\alpha}\omega_2 + 0.01290\omega_1\omega_2 - 0.008760\omega^2_2 + 3.585\delta_{H-N} + 3679.6\delta^2_{H-N}$$

$$\sigma_{xx} = 114.9 + 0.002260\,\phi_{C\alpha-C'-O} + 0.008908\,\phi^2_{C\alpha-C'-O} - 0.1384\,\phi_{C\alpha-C'-N} + 0.0231\,\phi_{C\alpha-C'-O}\phi_{C\alpha-C'-N} + 0.008900\,\phi^2_{C\alpha-C'-N} - 86.01\delta_{C\alpha-C'} + 0.3202\,\phi_{C\alpha-C'-O}\delta_{C\alpha-C'} + 0.3865\,\phi_{C\alpha-C'-N}\delta_{C\alpha-C'} + 556.8\delta^2_{C\alpha-C'} - 57.29\delta_{C'-O} + 0.4563\,\phi_{C\alpha-C'-O}\delta_{C'-O} + 0.4272\,\phi_{C\alpha-C'-N}\delta_{C'-O} - 22.11\delta_{C\alpha-C'}\delta_{C'-O} + 556.7\delta^2_{C'-O} - 24.31\delta_{C'-N} - 0.07056\,\phi_{C\alpha-C'-O}\delta_{C'-N} + 23.15\,\phi_{C\alpha-C'-N}\delta_{C'-N} + 20.46\delta_{C\alpha-C'}\delta_{C'-N} - 18.43\delta_{C'-O}\delta_{C'-N} + 556.7\delta^2_{C'-N} + 0.4289\,\phi_{C'-N-H} + 0.01129\,\phi^2_{C'-N-H} - 0.2086\,\phi_{C'-N-C\alpha} + 0.01119\,\phi_{C'-N-H}\phi_{C'-N-C\alpha} + 0.01129\,\phi^2_{C'-N-C\alpha} + 0.0002201\omega_1 - 0.00001916\,\phi_{C'-N-H}\omega_1 - 0.0003624\omega^2_1 - 0.00006991\omega_2 + 0.00001043\,\phi_{C'-N-H}\omega_2 - 0.00001030\,\phi_{C'-N-C\alpha}\omega_2 - 0.0007965\omega_1\omega_2 - 0.0003624\omega^2_2 - 18.17\delta_{H-N} - 1863\delta^2_{H-N}$$

$$\cos\theta = 0.8275 + 0.004759\,\phi_{C\alpha-C'-O} - 0.00005065\,\phi^2_{C\alpha-C'-O} + 0.007082\,\phi_{C\alpha-C'-N} - 0.0001589\,\phi_{C\alpha-C'-O}\phi_{C\alpha-C'-N} - 0.00005064\,\phi^2_{C\alpha-C'-N} - 0.1624\delta_{C\alpha-C'} + 0.004840\,\phi_{C\alpha-C'-O}\delta_{C\alpha-C'} + 0.005183\,\phi_{C\alpha-C'-N}\delta_{C\alpha-C'} - 3.166\delta^2_{C\alpha-C'} + 0.08732\delta_{C'-O} - 0.008226\,\phi_{156}\delta_{C'-O} - 0.004423\,\phi_{C\alpha-C'-N}\delta_{C'-O} + 0.4764\delta_{C\alpha-C}\delta_{C'-O} - 3.165\delta^2_{C'-O} + 0.01361\delta_{C'-N} + 0.002078\,\phi_{C\alpha-C'-O}\delta_{C'-N} - 0.02512\,\phi_{C\alpha-C'-N}\delta_{C'-N} - 0.3057\delta_{C\alpha-C}\delta_{C'-N} + 0.6169\delta_{C\alpha-C}\delta_{C'-N} - 3.166\delta^2_{C'-N} + 0.005044\,\phi_{C'-N-H} - 0.0002574\,\phi^2_{C'-N-H} - 0.0004384\,\phi_{C'-N-C\alpha} - 0.0001424\,\phi_{C'-N-H}\phi_{C'-N-C\alpha} - 0.0002574\,\phi^2_{C'-N-C\alpha} + 0.00001174\omega_1\omega_2 + 0.04544\delta_{H-N} + 1.2443\delta^2_{H-N}$$

$$\sin\zeta = -0.002726 + 0.000272\,\phi_{C\alpha-C'-O} + 0.0001164\,\phi_{C\alpha-C'-N} - 0.00002117\,\phi_{C\alpha-C'-O}\phi_{C\alpha-C'-N} + 0.008035\delta_{C\alpha-C'} - 0.00001797\,\phi_{C\alpha-C'-O}\delta_{C\alpha-C'} + 0.0001132\,\phi_{C\alpha-C'-N}\delta_{C\alpha-C'} - 0.3834\delta^2_{C\alpha-C'} + 0.008639\delta_{C'-O} - 0.0002885\,\phi_{C\alpha-C'-O}\delta_{C'-O} + 0.00008632\,\phi_{C\alpha-C'-N}\delta_{C'-O} - 0.03176\delta_{C\alpha-C}\delta_{C'-O} - 0.3834\delta^2_{C'-O} + 0.003239\delta_{C'-N} - 0.0004268\,\phi_{C\alpha-C'-O}\delta_{C'-N} - 0.0003629\,\phi_{C\alpha-C'-N}\delta_{C'-N} - 0.02459\delta_{C\alpha-C}\delta_{C'-N} - 0.0009177\delta_{C'-O}\delta_{C'-N} - 0.3835\delta^2_{C'-N} - 0.00003414\,\phi_{C'-N-H} - 0.00001785\,\phi^2_{C'-N-H} + 0.00003211\,\phi_{C'-N-C\alpha} - 0.00001785\,\phi^2_{C'-N-C\alpha} + 0.0008063\omega_1 - 0.00003418\,\phi_{C'-N-H}\omega_1 + 0.00001094\,\phi_{C'-N-C\alpha}\omega_1 - 0.0006962\omega_2 + 0.00002932\,\phi_{C'-N-H}\omega_2 + 0.001821\delta_{H-N} + 0.004610\delta^2_{H-N}$$

[a] The values at the beginning of each line correspond to the computed CSA variables of the reference conformation of DFT minimized NMA. The distances δ [Å], angles ϕ [°] and dihedrals ω [°] are the deviations of the atomic parameters from their equilibrium positions as defined in Figure 1 and listed in Table 1.

CSA direction were predicted from the quadratic equations obtained (listed in Table 2). The corresponding DFT values were also computed.

Figures 4a–fshow the comparison of the model-predicted and DFT-computed chemical shielding parameters for the 20 snapshots. Table 4 shows the statistical analysis of the comparisons. It is seen that the predicted values are well-correlated with the DFT values. We also observe that the ζ variations are very small in both cases (standard deviation 0.26° around an average of 0.1°). We thus conclude that the CSA tensor axes σ_{zz} and σ_{yy}, to a very good approximation, stay in the peptide plane for all conformations considered.

The correlations between computed and predicted values for the $^{13}C'$ CSA principal values indicate that the level of theory used is reasonable. We have also investigated whether the space of ten partially coupled parameters is sufficient for the description of the $^{13}C'$ CSA in this particular molecule.

As shown in Table 1 and in the empirical equations in Table 2, the CSA variations are dominated by variations in bond lengths and angles involving the C′ atom itself. Nevertheless, we feel that it is important to also consider the effects of the bond lengths, bond angles, and dihedral angles involving the N atom. Recent DFT and NMR studies show that the N atom can pyramidalize.[16,17] Most common is symmetric pyramidalization, in which the dihedral angles ω_1 and ω_2 (see definition in Figure 1) vary in opposite directions. These "butterfly motions" are predicted to amount to 30° at room temperature; at the same time, the Bell peptide plane dihedral ω, defined as $(\omega_1+\omega_2)/2$ stays at 180°.[18] Under these motions, the atoms Cα, C′, O and N stay in a single plane to very good approximation. The influence of the geometry around the N atom on the C′ CSA is, as indicted in Tables 1 and 2, of second order. These are the deviations in σ_{zz}; the deviations in other quantities are even smaller. Consequently, we suggest that our parameterization of the $^{13}C'$ CSA is also valid for MD snapshots generated with forcefields that keep the NH bond vector artificially in the peptide plane [such as chemistry Harvard molecular mechanics (CHARMM)[19] and Amber[20]].

Since the effects of H-bond variations on the $^{13}C'$ CSA are small (see Figure 3), we have not carried out any independent validation for this parameter.

Comparison with Experimental Values

NMR carbonyl CSA tensors have traditionally been determined from single-crystal peptide solid-state NMR spectra. More recently, several groups have calculated the CSA tensor using DFT methods.[9,15] Currently, workers are trying to determine experimental CSA tensors from cross-correlated NMR relaxation data.[5,10]

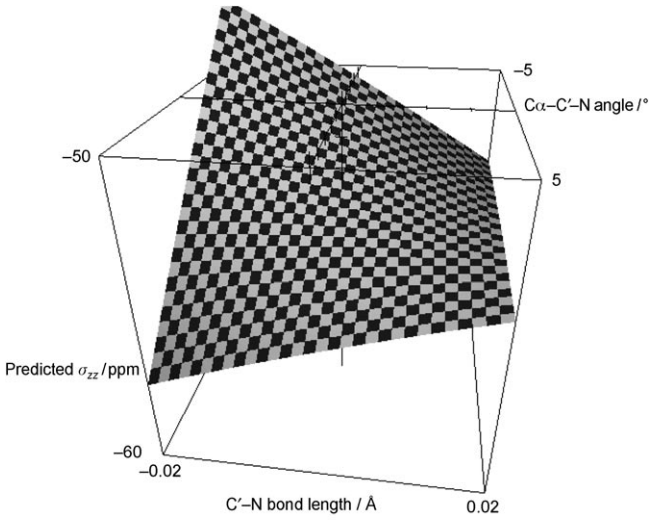

Figure 2. Illustration of a two-dimensional cross section through the hyper-dimensional parameter surface given in Table 2. Shown is the dependence of the 13C′ σ_{zz} CSA component on joint $\Phi_{C\alpha-C'-N}$ and $\delta_{C'-N}$ variations.

Table 3. Empirical parametric equations describing the $^{13}C'$ CSA dependence on H-bond parameters in NMA_2.[a]

$\sigma_{zz} = \sigma_{zz0} + 93.3132\exp(-1.2596\delta_{O-N})$
$\sigma_{yy} = \sigma_{yy0} - 92.2386\exp(-0.9751\delta_{O-N})$
$\sigma_{xx} = \sigma_{xx0} + 4.2368\exp(-1.0968\delta_{O-N})$

[a] σ_{zz0}, σ_{yy0}, and σ_{xx0} correspond to the values of the σ_{zz}, σ_{yy}, and σ_{xx} components in the absence of any hydrogen bond, as shown in Table 2. The distance δ_{O-N} is the O–N hydrogen-bond distance [Å].

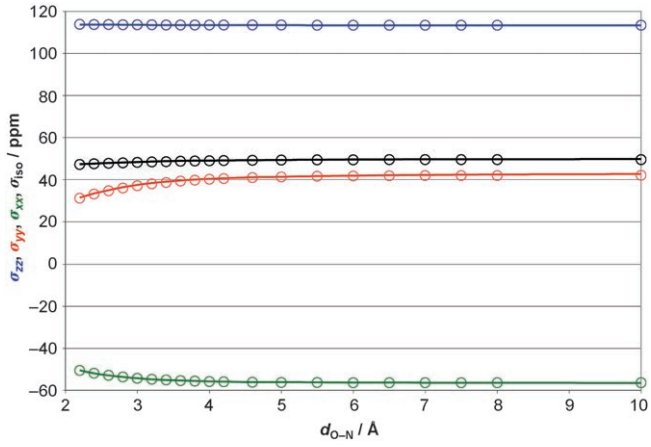

Figure 3. Parameterization of the effect of hydrogen-bond length on the $^{13}C'$ CSA principal values. Symbols are points obtained from the DFT calculations; the drawn lines are the parameterizations according to Table 3 ($\sigma_{zz0} = 113.45$, $\sigma_{yy0} = 42$, and $\sigma_{xx0} = -56.4$ ppm).

Herein, we use the parameterization to compute dynamic values of the CSA parameters σ_{zz}, σ_{yy}, σ_{xx} and $P_2(\cos\theta_{zz})$. From the 1 ns CHARMM trajectory on calmodulin in explicit solvent, we obtain a dynamic average for $\sigma_{zz}-\sigma_{xx}$ of 165.6 ppm with a dynamic root mean square deviation (RMSD) of 8 ppm

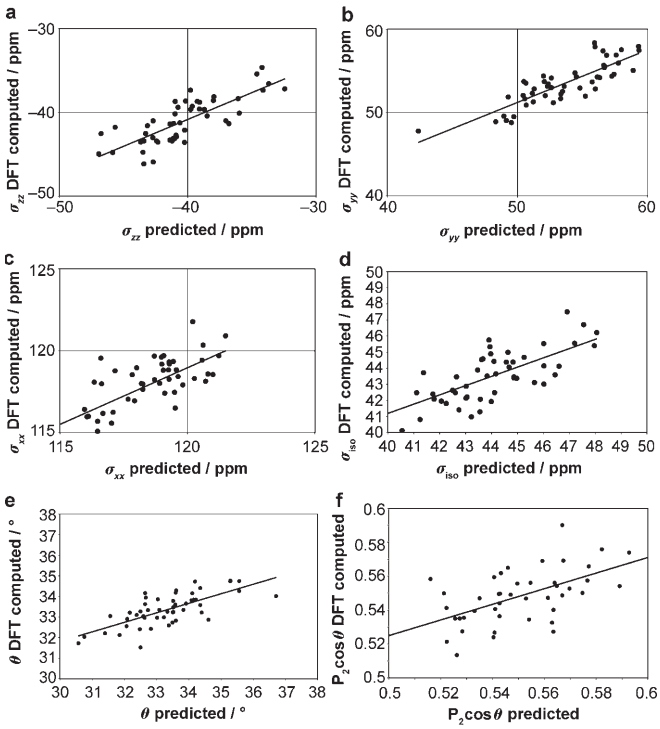

Figure 4. Correlation diagrams of the $^{13}C'$ CSA tensor variables for 20 molecular dynamics snapshots of NMA as predicted from the parameterization equations in Table 2 (abscissa) and as obtained from full DFT computations (ordinate) on the same molecules. a) σ_{zz}; b) σ_{yy}; c) σ_{xx}; d) σ_{iso}; e) θ; f) $P_2\cos\theta$. The lines are least-squares regressions; the statistics of these fits is listed in Table 4.

Table 4. Comparison of predicted and calculated C′ CSA parameters for 20 models of NMA taken from a MD run.[a]

Parameter	Range	RMSD[b] of fit	Regression (R^2)
σ_{zz}	14.5 ppm	1.72 ppm	0.61
σ_{yy}	17.0 ppm	1.50 ppm	0.71
σ_{xx}	6.8 ppm	1.19 ppm	0.41
σ_{iso}	9.8 ppm	1.19 ppm	0.54
$CSA = \sigma_{zz} - (\sigma_{yy}+\sigma_{xx})/2$	9.9 ppm	1.13 ppm	0.68
$\sigma_{zz}-\sigma_{xx}$	13.8 ppm	1.40 ppm	0.65
$\sigma_{yy}-\sigma_{xx}$	9.5 ppm	1.91 ppm	0.70
θ	6.1°	0.67°	0.51
$P_2\cos\theta$	0.08	0.016	0.51

[a] Also shown in Figure 4; all calculations were performed at the B3PW91/6-31G level; [b] RMSD = root mean square deviation.

(Table 5). This result should be compared with an average of 153.3 ppm from solid-state NMR experiments.[4,21] Bodenhausen and co-workers find 152.8–178 ppm in solution, depending on the motional model used, where the smallest number represents the value for the most dynamical model.[10]

We obtain for θ_{zz} an average value of 35°, with a dynamic RMSD of 3°, which compares well to the experimental values of Bodenhausen and co-workers, who obtained a spread of values between 35–37°.[10] Because of the excellent correspondence between our simulation data and the experimentally determined values, we conclude that our $^{13}C'$ CSA parame-

Table 5. Statistics of dynamical CSA fluctuations of 50 residues of calmodulin computed from a CHARMM–MD run using Table 2

	σ_{zz} [ppm]	σ_{yy} [ppm]	σ_{xx} [ppm]	σ_{iso} [ppm]	CSA[a] [ppm]	$\sigma_{zz}-\sigma_{xx}$ [ppm]	θ [°]
Residue average	−48.8	+54	116.9	40.95	134	165.6	35.06
Residue RMSD[b]	0.79	1.9	0.82	0.62	1.19	0.45	0.57
Residue range	±1.75	±5.18	±2.0	±1.05	±2.9	±1.0	±1.44
Dynamical RMSD	10.0	8.7	4.66	6.15	7.45	7.8	3.0
Dynamical range	±42	±33.3	±18.5	±22.4	±26.5	±27.8	±10.7

[a] Computed as $\sigma_{zz}-(\sigma_{yy}+\sigma_{xx})/2$; [b] RMSD = root mean square deviation.

terizations, calibrated for NMA, are also valid for the $^{13}C'$ nucleus in proteins and peptides in solution.

Intermezzo: Fundamental Considerations on CSA Relaxation

Herein, we want to assess the effect of the computed shielding fluctuations on the T_1 and T_2 relaxation of the $^{13}C'$ nucleus. In proteins, the $^{13}C'$ relaxation is dominated by the CSA relaxation, which originates from time fluctuations of the local magnetic field at the nucleus, which are caused by molecular tumbling. We want to outline the framework in which we can compare the relaxation caused by the global process with the relaxation induced by the local fluctuations as calculated from the MD runs.

The relaxation of the density matrix $\tilde{\sigma}(t)$ of spin I (the density matrix describes the state of the system) caused by a fluctuating interaction $H(t)$ between spin I and magnetic field B [Eq. (1)]:

$$H(t) = \sum_{m=-1}^{+1} F_m(t) T_m(I,B) \tag{1}$$

is given by Equation (2):[22]

$$\frac{d\tilde{\sigma}(t)}{dt} = -\frac{1}{2}\sum_{m=-1}^{m=+1}\left\{T_m(I,B),\left[T_m^{\dagger}(I,B),(\tilde{\sigma}(0)-\tilde{\sigma}_{eq})\right]\right\} \times \int_{t=0}^{t=\tau}\int_{-\infty}^{\infty} F_m^*(t)F_m(t+\tau)e^{i\omega_m\tau}dtd\tau \tag{2}$$

where the terms $T_m(I,B)$ are time-independent spin operators describing the interaction of the spin I with the magnetic field B, where the terms F_m describe the time dependence of the interaction, and where time τ is a time increment much smaller than the overall time dependence t.

We recognize the integral as the autocorrelation function, Equation (3):

$$AC(\tau) \equiv \left\langle F_m^*(t)F_m(t+\tau)\right\rangle_t, \tag{3}$$

written as the spectral density $J(\omega_m)$ [Eq. (4)]

$$J(\omega_m) \equiv 2\int_{\tau=2}^{\tau=\infty} AC(\tau)e^{-i\omega_m\tau}d\tau \cong 2\int_{\tau=0}^{\tau=\infty}\left\langle F_m^2\right\rangle e^{-\tau/\tau_c}e^{-i\omega_m\tau}d\tau = \sqrt{\frac{2}{\pi}}\left\langle F_m^2\right\rangle\frac{\tau_c}{1+(\omega_m\tau_c)^2} \tag{4}$$

where we used the common approximation that the autocorrelation function decays exponentially with correlation time τ_c.[1]

The $^{13}C'$ relaxation rates are proportional to $\left\langle F_m^2\right\rangle$ and to the spectral density at the transition frequency ω_c for T_1 relaxation and at frequencies ω_c and 0 for T_2 relaxation [Eqs. (5) and (6)]:[22]

$$\frac{1}{T_1^{CSA}} = \text{Constant} \times 6J(\omega_c) \tag{5}$$

$$\frac{1}{T_1^{CSA}} = \text{Constant} \times \{4J(0)+3J(\omega_c)\} \tag{6}$$

For tumbling-induced CSA relaxation, the functions F_m are given by time fluctuations of the shielding δ:[23]

$$\delta(t) = \frac{A}{2}\left[3\cos^2\theta(t) - 1 - R\sin^2\theta(t)\cos(2\phi(t))\right] \tag{7}$$

where $\theta(t)$ and $\phi(t)$ are the polar angles describing the direction of the external magnetic field, as seen from the CSA principle axis frame with principal values σ_{zz}^{PAS}, σ_{yy}^{PAS}, and σ_{xx}^{PAS}.

A is the axial term [Eq. (8)]:

$$A = \frac{2}{3}\left[\sigma_{zz}^{PAS} - \left(\frac{\sigma_{xx}^{PAS}+\sigma_{yy}^{PAS}}{2}\right)\right] \tag{8}$$

and R is the rhombic term [Eq. (9)]:

$$R = \frac{\sigma_{yy}^{PAS}-\sigma_{xx}^{PAS}}{\sigma_{zz}^{PAS}-\sigma_{iso}} \tag{9}$$

and where [Eq. (10)]:

$$\sigma_{iso} = (\sigma_{zz}^{PAS}+\sigma_{yy}^{PAS}+\sigma_{xx}^{PAS})/3 \tag{10}$$

For an axially symmetric CSA, Equation (7) simplifies to Equation (11):

$$\delta(t) = \frac{A}{2}[3\cos^2\theta(t) - 1], \quad (11)$$

which is proportional to the spherical harmonic $Y_0^2(\theta)$.

The averages of the spherical harmonics are known; averaging Equation (11) over isotropic space ($\theta(t)$,$\phi(t)$) yields Equation (12):

$$\langle\delta(t)\delta^*(t)\rangle = \frac{A^2}{5} \quad (12)$$

For example, for an axially symmetric CSA with $\sigma_{zz}=$ 100 ppm and $\sigma_{yy}=\sigma_{xx}=-50$ ppm, a power term of 2000 ppm^2 is obtained.

The situation is more complicated for a rhombic CSA such as is the case for the $^{13}C'$ nucleus. Numerical integration of Equation (7) over isotropic space ($\theta(t)$,$\phi(t)$) for $\sigma_{zz}=-89$, $\sigma_{yy}=$ 10, and $\sigma_{xx}=79$ ppm (see leading terms in Table 2, with the isotropic value of 36 ppm subtracted) yields a power term of 1940 ppm^2.

Adopting the common assumption that the overall motions and the peptide-plane distortions are statistically uncorrelated, their joint correlation function can be written as the product of the individual correlation functions.[2,3] This procedure leads to an expression analogous to the model-free approximation [Eq. (13)]:[2,3]

$$\mathrm{AC}(\tau) = \left(\frac{\langle F_m^{\mathrm{global}} F_m^{*\mathrm{global}}\rangle}{\langle F_m^{\mathrm{global}} F_m^{*\mathrm{global}}\rangle + \langle F_m^{\mathrm{local}} F_m^{*\mathrm{local}}\rangle} + \frac{\langle F_m^{\mathrm{local}} F_m^{*\mathrm{local}}\rangle}{\langle F_m^{\mathrm{global}} F_m^{*\mathrm{global}}\rangle + \langle F_m^{\mathrm{local}} F_m^{*\mathrm{local}}\rangle}\exp(-\tau_{\mathrm{local}}/\tau)\right)\exp(-\tau_{\mathrm{R}}/\tau) \quad (13)$$

with the spectral density

$$J_m(\omega) = 2\int_{\tau=0}^{\infty}\cos(\omega\tau)\mathrm{AC}(\tau)d\tau = 2\left\{\frac{\langle F_m^{\mathrm{global}} F_m^{*\mathrm{global}}\rangle}{\langle F_m^{\mathrm{global}} F_m^{*\mathrm{global}}\rangle + \langle F_m^{\mathrm{local}} F_m^{*\mathrm{local}}\rangle}\frac{\tau_{\mathrm{R}}}{1+\omega^2\tau_{\mathrm{R}}^2} + \frac{\langle F_m^{\mathrm{local}} F_m^{*\mathrm{local}}\rangle}{\langle F_m^{\mathrm{global}} F_m^{*\mathrm{global}}\rangle + \langle F_m^{\mathrm{local}} F_m^{*\mathrm{local}}\rangle}\frac{\tau}{1+\omega^2\tau^2}\right\} \quad (14)$$

where

$$\tau = \frac{\tau_{\mathrm{local}}\tau_{\mathrm{R}}}{\tau_{\mathrm{local}} + \tau_{\mathrm{R}}} \quad (15)$$

with the correlation times τ_{R} and τ_{local} referring to global and local motion, respectively.

The terms $\frac{\langle F_m^{\mathrm{global}} F_m^{*\mathrm{global}}\rangle}{\langle F_m^{\mathrm{global}} F_m^{*\mathrm{global}}\rangle + \langle F_m^{\mathrm{local}} F_m^{*\mathrm{local}}\rangle}$ and $\frac{\langle F_m^{\mathrm{local}} F_m^{*\mathrm{local}}\rangle}{\langle F_m^{\mathrm{global}} F_m^{*\mathrm{global}}\rangle + \langle F_m^{\mathrm{local}} F_m^{*\mathrm{local}}\rangle}$ can be associated with order parameters S^2 and $(1-S^2)$, respectively.

Finally, the CSA relaxation due to the combined presence of local distortions and global tumbling is obtained by substituting Equation (14) into Equations (5) and (6).

The Effects of Dynamical CSA Variation on $^{13}C'$ NMR Relaxation

We use the parameterization in Table 2 to compute dynamic values of the CSA parameters σ_{zz}, σ_{yy}, σ_{xx} and $P_2\cos\theta_{zz}$. Tables 6 and 7 list the results for a 1 ns CHARMM trajectory of Ca^{2+}-saturated calmodulin (a 140-residue protein) in an explicit solvent of 10000 water molecules. Large variations are found for the individual principal axis values of the $^{13}C'$ tensor, with the largest variations found for σ_{zz}. The angle θ_{zz}, defined as the angle of the CSA principal axis σ_{zz} with the C′–N bond, also varies substantially. The angle ζ fluctuates little, showing that the $^{13}C'$ CSA tensor axes σ_{zz} and σ_{yy} remain in the peptide plane during the simulation. Little difference is obtained for a residue in an α-helix (plane 10–11; Table 6) or a residue in dynamic random coil (plane 79–80; Table 7).

Table 8 lists corresponding results from a 10 ns CHARMM trajectory of Ca^{2+}-saturated calmodulin in implicit solvent. This calculation was carried out to investigate if long-term fluctuations, which are not captured on the 1 ns timescale, are present at the 10 ns timescale. This latter time scale represents a lower limit on local fluctuations that may affect NMR relaxation. The close correspondence of Tables 6 and 8 shows that long-term fluctuations are not present in this simulation; hence, the MD simulations in explicit water at 1 ns are sufficient for the current analysis.

Figures 5a and b show the autocorrelation functions of CSA parameters σ_{zz}, σ_{yy}, σ_{xx}, and $P_2\cos\theta_{zz}$ in the 1 ns simulation of calmodulin. We estimate 3 ps for τ_{local} from these plots, and obtain, for the largest fluctuations, $<\delta\sigma_{zz}{}^2>=100$ ppm^2 and $<P_2\cos\theta_{zz}{}^2>=0.006$ units.

Table 6. CHARMM–MD for calmodulin plane 10–11 with 10000 water 303 K.[a]

	σ_{zz} [ppm]	$\delta\sigma_{zz}{}^2$ [ppm^2]	σ_{yy} [ppm]	σ_{xx} [ppm]	θ [°]	$P_2\cos\theta$	$\delta(P_2\cos\theta)^2$	ζ [°]
Average	−49.76	86.71	54.93	114.96	35.49	0.49	0.0054	−0.27
Standard deviation	9.34	127.04	7.89	4.02	3.00	0.07	0.0072	0.45
Maximum	22.57	929.23	28.45	12.47	7.46	0.17	0.0304	1.47
Minimum	−31.87	−86.71	−16.72	−9.85	−7.25	−0.19	−0.0054	−1.63
τ_{local} [ps]	3		3	3	3	3		3

Calculated values of the $^{13}C'$ CSA components of peptide, plane 10–11 (helix) over a 1 ns MD calculation, of Ca^{2+}-saturated calmodulin with 10000 solvent molecules, evaluating every 5 ps using the empirical CSA parameterizations listed in Table 2

Table 7. CHARMM–MD for calmodulin plane 79–80 with 10000 water molecules.[a]

	σ_{zz} [ppm]	$\delta\sigma_{zz}^2$ [ppm^2]	σ_{yy} [ppm]	σ_{xx} [ppm]	θ [°]	$P_2\cos\theta$	$\delta(P_2\cos\theta)^2$	ζ [°]
Average	−48.21	89.41	55.23	117.45	34.23	0.52	0.0049	−0.31
Standard deviation	9.48	115.51	8.82	4.99	2.88	0.07	0.0077	0.46
Maximum	23.01	440.04	26.68	14.14	9.55	0.13	0.0536	1.45
Minimum	−22.81	−89.39	−18.01	-14.90	−5.51	−0.24	−0.0049	−1.70
τ_{local} [ps]	3		3	3	3	3		3

[a] Calculated values of the $^{13}C'$ CSA components of peptide, plane 79–80 (coil) over a 1 ns molecular dynamics calculation, of Ca^{2+}-saturated calmodulin with 10000 solvent molecules, evaluating every 5 ps using the empirical CSA parameterizations listed in Table 2

Table 8. CHARMM–MD for Calmodulin plane 10–11 with implicit water at 303 K.[a]

	σ_{zz} [ppm]	$\delta\sigma_{zz}^2$ [ppm^2]	σ_{yy} [ppm]	σ_{xx} [ppm]	θ [°]	$P_2\cos\theta$	$\delta(P_2\cos\theta)^2$	ζ [°]
Average	−48.91	99.69	52.75	116.63	34.67	0.51	0.0054	−0.38
Standard deviation	9.99	144.66	8.48	4.58	3.01	0.07	0.0081	0.45
Maximum	34.11	1063.69	39.83	22.89	10.66	0.22	0.0685	1.64
Minimum	−32.84	−99.69	−27.91	−19.22	−9.76	−0.27	−0.0054	−1.97
τ_{local} [ps]	<5		<5	<5	<5	<5		<5

[a] Calculated values of the 13C′ CSA components of peptide plane 10–11 over a 10 ns molecular dynamics calculation of Ca^{2+}-saturated calmodulin, using implicit solvent, evaluating every 5 ps using the empirical CSA parameterizations listed in Table 2.

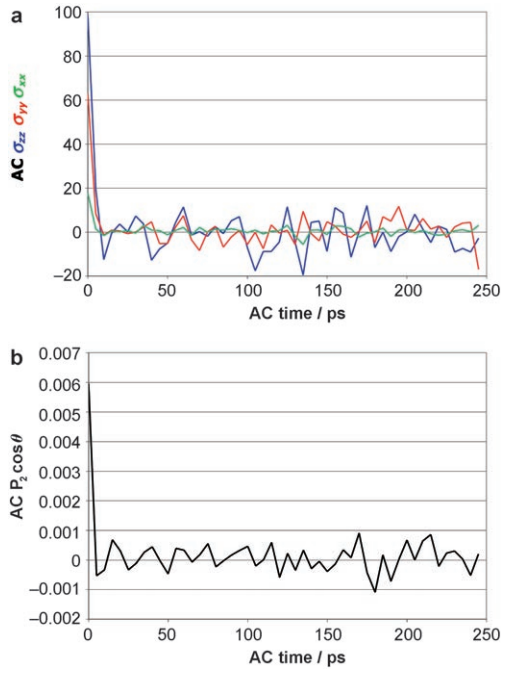

Figure 5. Autocorrelation functions for the NMR shielding parameters of the $^{13}C'$ nucleus of residue 10 in the 1 ns CHARMM–MD simulation of calmodulin in explicit solvent. a) $<(\sigma_{zz})_t(\sigma_{zz})_{t+\tau}>$, $<(\sigma_{yy})_t(\sigma_{xx})_{t+\tau}>$, and $<(\sigma_{yy})_t(\sigma_{yy})_{t+\tau}>$; b) $<P_2\cos(\theta_{zzt}-\theta_{zzt+\tau})>$.

The effect of the fluctuation of the tensor principal axis $<P_2\cos\theta_{zz}{}^2>$ on $^{13}C'$ NMR relaxation as compared to the overall tumbling is readily computed. As shown in Equation (12), a complete spherical averaging of $P_2\cos\theta_{zz}{}^2$ yields 0.2 units. Hence, we find a value of 0.006/0.2 = 0.03 for the ratio of the effect of the local variations and the global tumbling. Inserting these values in Equation (14), we find Equation (16):

$$J_m(\omega) = 0.97\frac{\tau_R}{1+\omega^2\tau_R^2} + 0.03\frac{\tau}{1+\omega^2\tau^2} \quad (16)$$

With the value for τ_{local} of 3 ps, Equation (16) can be truncated to Equation (17):

$$J_m(\omega) = 0.97\frac{\tau_R}{1+\omega_m^2\tau_R^2} \quad (17)$$

for all relevant values of τ_R (>5 ns) and of ω_m (0 or $>125\times2\pi$ MHz). Hence, the local angle fluctuations reduce both $1/T_1$ and $1/T_2$ by just 3%.

For the calmodulin simulation, $<\delta\sigma_{zz}{}^2> = \langle F_m^2\rangle A^2 \cong 100$ ppm^2. Comparing this with the value of $\langle F_m^2\rangle A^2 = 1940$ ppm^2 for isotropic fluctuations of the rhombic CSA tensor (see above), we obtain $S^2 = 1940/2040 = 0.95$, and we may write Equation (18) for Equation (14):

$$J_m(\omega) = 0.95\frac{\tau_R}{1+\omega^2\tau_R^2}, \quad (18)$$

which represents a 5% decrease in both $1/T_1$ and $1/T_2$.

Significant fluctuations occur in hydrogen-bonding lengths in the first helix of calmodulin. Using the parameterization in Table 3, we compute the fluctuations in $^{13}C'$ CSA caused by these effects. These fluctuations have very long correlation times (about 300 ps, Figure 6). However, since the fluctuations themselves are very small (Table 9), there is no noticeable effect on the $^{13}C'$ relaxation.

Table 9. CHARMM–MD for calmodulin residue 8 H-bonded to residue 12.[a]

	d_{O-N} [Å]	$\delta\, d_{O-N}$ [Å]	σ_{zz} [ppm]	$\delta\sigma_{zz}^2$ [ppm^2]	σ_{yy} [ppm]	σ_{xx} [ppm]
Average	3.23	0.43	−53.98	3.03	37.28	113.60
Standard deviation	0.75	0.75	1.74	3.49	3.12	0.12
Maximum	2.08	2.08	4.72	19.24	4.96	0.31
Minimum	−1.50	−1.50	−2.60	−3.03	−8.28	−0.17
τ_{local} [ps]			350		350	350

[a] Calculated fluctuations of the $^{13}C'$ CSA components for calmodulin residue 8 H-bonded to residue 12 as a result of hydrogen bond length (d_{O-N})variations over 10 ns in a CHARMM MD run, evaluating every 5 ps (303 K). We use the parameterization in Table 3.

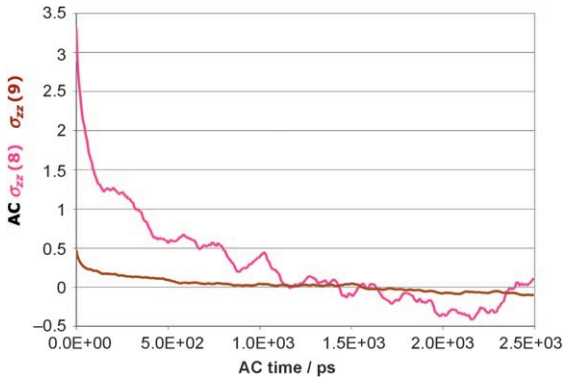

Figure 6. Autocorrelation functions for the NMR shielding parameters of the $^{13}C'$ nucleus of residues 8 and 9 in the 10 ns CHARMM–MD simulation of calmodulin due to variations in the H-bonding length with residues 11 and 12, respectively.

In order to investigate whether the fluctuations are similar in a β-sheet protein, we carried out CHARMM–MD simulations of the small protein GB3. The results are very similar to those obtained for calmodulin (shown in summary in Table 12).

In order to investigate in more detail the small but significant 5% loss of correlation in the first few picoseconds of the CHARMM dynamics, we carried out extensive MD calculations using an quantum mechanically correct spectroscopically determined force field (SDFF) at 40 and 220 K.[16,17,24] This force field accurately computes, amongst other parameters, the frequencies and intensities of peptide vibrational IR spectra. Hence, this force field is a force field of choice to best characterize the early events in the correlation functions of proteins. Regretfully, this force field is not yet fully parameterized for amino acids. Therefore, we computed an MD trajectory for a planar NMA trimer in vacuo, in which the central NMA is hydrogen bonded to both of its neighbors.

Table 10 shows the relevant data, which are found to be remarkably similar to the results obtained for the CHARMM–MD runs for complete proteins. However, Figure 7 shows that the correlation functions are highly oscillatory. Nevertheless, we may still extract $<\delta\sigma_{zz}^2> = 100$ ppm^2 with a τ_{local} of 1 ps and $<P_2\cos\theta_{zz}^2>$ of 0.006 units with a τ_{local} of 100 ns. For the angular perturbation, we compute a scaling factor of 0.97 for the bond-length variations.

Figure 7 shows damped periodic oscillations in the autocorrelation functions. Can these fluctuations cause NMR relaxation? Fourier transformation of the CSA fluctuations discloses five major frequency components, which are listed in Table 11. The frequencies correspond closely to the amide bands that are detected in IR spectra of peptides. In addition, the assignments of the different IR bands also correspond to the fluctuating parameters. These results are not surprising, since the SDFF was designed to reproduce IR data.

We thus find that the frequencies of these oscillations are much too high to drive NMR transitions; it would require magnets that allow ^{13}C frequencies in the hundreds of GHz.

Correlations Between the Scaling Factors

Above, we computed the relaxation scaling factors caused by fluctuations in σ_{zz} and $P_2\cos\theta_{zz}$ only; σ_{yy} and σ_{xx} fluctuate as well and will also cause a scaling, albeit a less effective one (see Table 12, which summarizes all scaling factors). The scaling factors of σ_{zz}, σ_{yy}, and σ_{xx} must not be multiplied together, because σ_{zz}, σ_{yy}, and σ_{xx} fluctuations occur by definition only when the PAS *zz*, *yy*, or *xx* axes coincide with the external field. In other words, when the PAS *zz* coincides with the external

Table 10. SDFF MD for NMA_3 central molecule in vacuo at 224 K.[a]

	σ_{zz} [ppm]	$\delta\sigma_{zz}^2$ [ppm^2]	σ_{yy} [ppm]	σ_{xx} [ppm]	θ [°]	$P_2\cos\theta$	$\delta(P_2\cos\theta)^2$	ζ [°]
Average	−45.67	110.45	53.33	118.04	37.68	0.44	0.00673	−0.32
Standard deviation	10.51	176.98	9.01	4.40	3.24	0.08	0.01062	1.32
Maximum	35.29	3138.61	58.29	60.22	16.16	0.27	0.16656	4.39
Minimum	−57.00	−110.45	−46.77	−23.49	−11.32	−0.42	−0.00673	−5.82
τ_{local} [ps]	20		20	20	20	3		

[a] Calculated values of the $^{13}C'$ CSA components of the central molecule of a tri-NMA β-sheet model over a 1 ns portion of a 10 ns molecular dynamics calculation with the SDFF force field, evaluating every 50 fs using the empirical CSA parameterizations listed in Table 2.

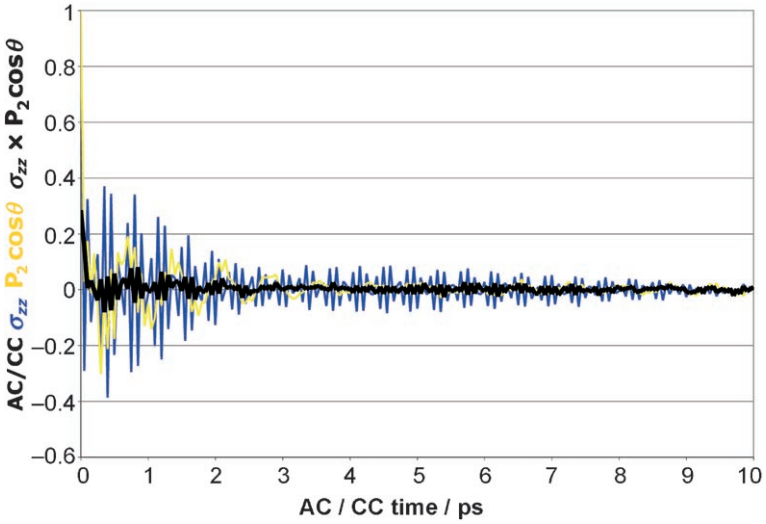

Figure 7. Normalized autocorrelation functions for the NMR shielding parameters $<(\sigma_{zz})_t(\sigma_{zz})_{t+\tau}>$ and $<P_2\cos(\theta_{zzt}-\theta_{zzt+\tau})>$ of $^{13}C'$ of the central NMA in the 1 ns SPEARS-MD simulation of NMA_3 in vacuo. The cross correlation function between these quantities is also shown.

field, σ_{zz} fluctuates but σ_{yy} and σ_{xx} do not. Intermediate angles will reduce the contributions of the individual scaling factors. We conclude that the effects of the σ_{zz} fluctuations, which are the largest fluctuations in all simulations, represent an upper limit to the CSA value scaling factors.

Oscillations of the in-plane angle of the σ_{zz} principal axis orientation (more accurately, $P_2\cos\theta_{zz}$) do occur simultaneously with fluctuations in σ_{zz} and σ_{yy} (not σ_{xx}, which is perpendicular to the peptide plane). Figure 7 shows that the σ_{zz} and $P_2\cos\theta_{zz}$ fluctuations occur at different time scales. This is underscored by the value of their cross correlation function, which has an amplitude of only 0.3, as compared to the normalized autocorrelation functions, which both have amplitude 1. We conclude that the angular and bond fluctuations are approximately statistically independent, so that their scaling factors must be multiplied.

Conclusions

We have demonstrated that the $^{13}C'$ CSA tensor principal values and orientation can be systematically parameterized with ten variables using hypersurfaces with up to five dimensions. The parameterized CSA values correlate with DFT-calculated CSA values for a test set of 20 molecular-dynamics snapshots of an NMA trimer. When applied to MD simulations of the proteins calmodulin and GB3 using the CHARMM forcefield, relatively large variations of ± 26, ± 22, and ± 10 ppm in $^{13}C'$ σ_{zz}, σ_{yy}, and σ_{xx}, respectively, are predicted, while the orientation of the $^{13}C'$ CSA σ_{zz} axis varies by $\pm 7^\circ$. Correlation function analysis indicates that these fluctuations occur at a sub-10 ps timescale, giving rise to a factor of 0.93 scaling of both the $1/T_2$ and $1/T_1$ relaxation rates.

Analysis of an MD computation on a β-sheet motif, using a quantum-mechanically correct SDFF, shows remarkably similar

Table 11. Discrete frequencies in the CSA modulation in the SPEARS MD for NMA_3.[a]

Period [s]	Frequency [Hz]	CSA terms	Geometrical terms	Frequency[b] [cm^{-1}]	IR band[b]
1.67E−12	6.00E+11	all	$\phi_{C'NH}$, ω_1, ω_2	20	–
1.15E−13	8.72E+12	σ_{yy}, P_2	$\phi_{C\alpha 1C'N}$, $\phi_{C'NC\alpha 2}$, $\phi_{C'NH}$, $\delta_{C'N}$	291 (≈200)	amide VII skeletal torsion
7.30E−14	1.37E+13	σ_{xx}	$\phi_{C\alpha C'N}$, $\phi_{C\alpha C'O}$, $\delta_{C'N}$	457	–
5.10E−14	1.96E+13	σ_{xx}	$\phi_{C\alpha C'O}$, $\phi_{C'NC\alpha 2}$, $\delta_{C\alpha C'O}$, $\delta_{C'N}$	653 (625–767)	amide IV OC′N bend
2.59E−14	3.86E+13	P_2	$\phi_{C\alpha C'O}$, $\phi_{C'NC\alpha 2}$, $\phi_{C'NH}$, $\delta_{C\alpha 1C'}$, $\delta_{C'N}$	1287 (1229–1301)	amide III C′N stretch
1.95E−14	5.14E+13	σ_{zz}, σ_{yy}, σ_{xx}	$\phi_{C'NC\alpha 2}$, $\phi_{C'NH}$, $\delta_{C\alpha 1C'}$, $\delta_{C'N}$, $\delta_{C'O}$	1713 (1600-1690)	amide I C′O stretch
1.07E−14	9.35E+13	σ_{yy}, σ_{xx}	δ_{NH}	3117 (≈3100)	NH stretch

[a] Central NMA molecule at 224 K. b) Frequencies in parentheses and assignments were taken from ref. [29].

Table 12. Summary of protein $^{13}C'$ relaxation scaling factors.

	CHARMM calmodulin[a]				CHARMM GB3[b]				SDFF NMA_3[c]			
	$\delta\sigma_{zz}^2$	$\delta\sigma_{yy}^2$	$\delta\sigma_{xx}^2$	$\delta(P_2)^2$ x1000	$\delta\sigma_{zz}^2$	$\delta\sigma_{yy}^2$	$\delta\sigma_{xx}^2$	$\delta(P_2)^2$ x1000	$\delta\sigma_{zz}^2$	$\delta\sigma_{yy}^2$	$\delta\sigma_{xx}^2$	$\delta(P_2)^2$ x1000
Average	87	62	16	5.4	106	75	25	5.2	110	81	19	6.7
τ_{local} [ps]	3	3	3	3	<50	<50	<50	<50	20	20	20	3
Scaling factor	0.96	0.97	0.99	0.97	0.95	0.96	0.99	0.97	0.95	0.96	0.99	0.97
Combined scaling factors[d]	0.93	0.94			0.92	0.93			0.92	0.93		
Maximum scaling factor	0.93				0.92				0.92			

[a] Peptide plane 10–11 at 303 K; [b] peptide plane 54–55 at 303 K; [c] central NMA at 224 K. [d] The combined scaling is the product with the $P_2\cos$ scaling factor, for σ_{zz} and σ_{yy} only (see text).

CSA fluctuations, leading to an overall 0.92 scaling factor for $1/T_2$ and $1/T_1$ ^{13}C relaxation.

Parameterization of the effect of hydrogen-bond length variations on the $^{13}C'$ CSA indicates that these effects can be completely neglected for $^{13}C'$ relaxation.

In total, our work demonstrates that $^{13}C'$ CSA relaxation is relatively little affected by large local distortions in bond lengths and angles (scaling factors 0.93). Importantly, the effects are the same whether the residues are in helices, in sheets, or in dynamic coils. Hence, variations in $^{13}C'$ CSA relaxation autocorrelation or cross correlation rates over a protein sequence are indicative of local motions of the entire peptide plane rather than variations in bond lengths and angles. This result is important, because it establishes that $^{13}C'$ relaxation is a valid tool for measurement of interesting dynamical events in proteins and can be used in conjunction with other relaxation vectors (such as NH) to derive models of anisotropic protein backbone plane dynamics. While this has been implicitly assumed by quite a few authors,[5–13] including ourselves, it is only in this study that it has been rigorously established.

Experimental Section

DFT Calculations and Parameterizations: The program Gaussian 03 (Gaussian, Inc., Carnegie, USA) was used with the B3PW91 functional and the 6–31G basis set, which is accurate enough for such a system.[25] The energy of the NMA molecule (Figure 1) was first minimized through geometry optimization. To accelerate convergence, the methyl groups were restrained from rotation.

The influence of changes in the bond lengths, bond angles, and dihedrals on the $^{13}C'$ CSA was then investigated by additional DFT calculations in which one geometry parameter at a time was varied (frozen) while relaxing the molecule with respect to all other coordinates (except methyl rotation). The gauge including atomic orbitals (GIAO) method was used in all CSA calculations.[26] Initially, it was determined which molecular parameters affect the CSA [defined as $\sigma_{zz}-(\sigma_{yy}+\sigma_{xx})/2$] by more than 0.5 ppm. Subsequently, molecular parameters were varied pairwise to determine the presence of covariance. Table 1 shows the results of these training calculations.

Parameters 9 and 10 are the dihedral angles describing the planarity of the peptide plane. The angle variations were constructed such that the atoms O, C′, Cα1, and N all remained in one plane. Differences in the angles ω_1 and ω_2 then describe out-of-plane motions of the NH and NCα2 vectors, caused by pyramidalization of the N atom (i.e. admixing sp^3 character in the sp^2-dominated wave functions).[16,17]

It was determined that the effects of the molecular parameters 1–5 on the $^{13}C'$ CSA were strongly correlated, as were the parameters 7–10. Parameter 6 was independent. Without further investigation, it was assumed that the principal values of the CSA tensor and the angles θ_{zz} and θ_{xx} of its principal axes, as defined in Figure 1, have the same covariance dependencies on the molecular parameters as the CSA defined above. Thus, it was decided to construct five five-dimensional hypersurfaces to parameterize the dependence of the C′ σ_{zz}, σ_{yy}, σ_{xx}, θ_{zz}, and θ_{xx} upon variables 1–5, five four-dimensional hypersurfaces to parameterize the dependence of the same five quantities upon variables 7–10, and five one-dimensional functions to parameterize the dependence of the same five quantities upon variable 6.

Using the program Mathematica 5.2 (Wolfram Research, Inc., Champaign, IL), the five-, four- and one-dimensional hypersurfaces were fitted against quadratic equations, which contained all parameters and their pair-wise cross terms as needed. The resulting fitting parameters are given in Table 2.

The parameterization of the hydrogen-bonding effect was carried out using a planar NMA_2 molecule, where the distance between the hydrogen acceptor O atom of molecule 1 and acceptor N atom of molecule 2 was systematically constrained between 2.2 and 10 A. The angles O···H–N and C–O···N were restrained at 180°. The program Gaussian 03 was used with the B3PW91 functional and 6–31G basis set. To accelerate the convergence, the methyl groups were restrained from rotations. The energy of the constrained NMA_2 molecule was minimized before the CSA of the $^{13}C'$ of molecule 1 (acceptor) was calculated. The program Mathematica 5.2 was used to obtain the parameterization of the DFT results as shown in Table 3.

Molecular Dynamics Simulations and $^{13}C'$ CSA Parameter Extraction: A 1 ns MD trajectory was calculated for Ca^{2+}-saturated calmodulin with 10000 TIP3 water molecules at 303 K. The trajectory was computed using the CHARMM software package.[27] The coordinates were saved every 5 ps. The system was equilibrated for 20 ps with the protein backbone held fixed and then for 40 ps with no restraints.

In addition, a 10 ns CHARMM molecular dynamics trajectory was calculated in implicit solvent using a generalized Born implicit solvent model,[28] using 2 fs steps. Other parameters were as above. The system was equilibrated for 100 ps.

A 10 ns CHARMM molecular dynamics trajectory was also calculated for GB3 in implicit solvent, using a generalized Born implicit solvent model,[28] using 2 fs steps. Other parameters were as above. The system was equilibrated for 100 ps.

A 10 ns molecular dynamics trajectory was calculated for a planar hydrogen-bonded trimer of NMA molecules at 223 K. Here we used the in-house developed SPEARS molecular modeling package (Palmo and Krimm, to be published) and a quantum mechanically based force field derived for the peptide plane with the SDFF method developed by Krimm and co-workers.[16] The SDFF correctly reproduces frequencies and amplitudes of IR spectra of peptide groups. Hence, the force field is accurate at short time scales.

The central molecule of NMA_3, which is hydrogen-bonded at both the C′ and NH functionalities, may be considered a model for amino acids in the interior of a protein β-sheet. In order to obtain a more realistic hydrogen-bond potential, the partial charges (bond charge increments) on the oxygen and amide hydrogen atoms were increased by about 14% from the vacuum values.[24] This increase represents the effects of intermolecular charge polarization that was not explicitly included in the force field. The dynamics of the NMA trimer were simulated in vacuo, which necessitated the use of soft torsion-type intermolecular constraints between the molecules to avoid cyclization and to keep the trimer flat on average. The 10 ns MD run (with a 0.5 fs time step) took 12 h of CPU time on the Macintosh G5 computer. Snapshots were saved for every 5 fs. During the calculation, the sum of potential and kinetic energy remained very stable at -240.52 ± 0.1 kcal mol^{-1}.

Computer programs, both in Python and Fortran 77 languages, were developed to extract the molecular parameters of interest from the individual snapshots of the molecular dynamics simulations, which predict the $^{13}C'$ CSA tensor parameters on the basis of the hypersurfaces listed in Table 1. Autocorrelation functions of the time-dependent tensor fluctuations were computed from these predicted values using another set of in-house written Fortran 77 programs. All correlation functions computed are independent of overall motional reorientations.

Acknowledgements

The majority of this work was supported by the National Science Foundation grant MCB 0135330. E.R.P.Z. was also partially supported through NIH R01 GM63027. I. A. acknowledges support from the NSF CAREER award. The authors thank Drs. S. Krimm, B. Mannfors, N. Mirkin (all U. Michigan) and Dr. D. Case (Scripps Research Institute, La Jolla, CA, USA) for stimulating discussions.

Keywords: chemical shift anisotropy · density functional calculations · molecular dynamics · NMR spectroscopy

[1] A. Abragam, *The Principles of Nuclear Magnetism*, Clarendon Press, Oxford, **1961**.
[2] G. Lipari, A. Szabo, *J. Am. Chem. Soc.* **1982**, *104*, 4546 – 4558.
[3] G. Lipari, A. Szabo, *J. Am. Chem. Soc.* **1982**, *104*, 4559 – 4570.
[4] M. W. F. Fischer, L. Zeng, A. Majumdar, E. R. P. Zuiderweg, *Proc. Natl. Acad. Sci. USA* **1998**, *95*, 8016 – 8019.
[5] Y. X. Pang, E. R. P. Zuiderweg, *J. Am. Chem. Soc.* **2000**, *122*, 4841 – 4842.
[6] Y. X. Pang, M. Buck, E. R. P. Zuiderweg, *Biochemistry* **2002**, *41*, 2655 – 2666.
[7] T.-Z. Wang, S. Cai, E. R. P. Zuiderweg, *J. Am. Chem. Soc.* **2003**, *125*, 8639 – 8643.
[8] T.-Z. Wang, K. K. Frederick, T. I. Igumenova, A. J. Wand, E. R. P. Zuiderweg, *J. Am. Chem. Soc.* **2005**, *127*, 828 – 829.
[9] P. R. Markwick, M. J. Sattler, *J. Am. Chem. Soc.* **2004**, *126*, 11 424 – 11 425.
[10] K. Loth, P. Pelupessy, G. Bodenhausen, *J. Am. Chem. Soc.* **2005**, *127*, 6062 – 6068.
[11] F. Cisnetti, K. Loth, P. Pelupessy, G. Bodenhausen, *ChemPhysChem* **2004**, *5*, 807 – 814.
[12] T. S. Ulmer, B. E. Ramirez, F. Delaglio, A. J. Bax, *Am. Chem. Soc.* **2003**, *125*, 9179 – 9191.
[13] S. L. Chang, N. Tjandra, *J. Mag. Reson.* **2005**, *174*, 43 – 53.
[14] T.-Z. Wang, D. S. Weaver, S. Cai, E. R. P. Zuiderweg, *J. Biomol NMR* **2006**, *36*, 79 – 102.
[15] X. P. Xu, D. A. Case, *Biopolymers* **2002**, *65*, 408 – 423.
[16] K. Palmo, B. Mannfors, N. G. Mirkin, S. Krimm, *Biopolymers* **2003**, *68*, 383 – 394.
[17] B. E. Mannfors, N. G. Mirkin, K. Palmo, S. Krimm, *J. Phys. Chem.* **2003**, *A107*, 1825 – 1832.
[18] B. P. Bell, *Trans. Faraday Soc.* **1945**, *41*, 293 – 295.
[19] B. R. Brooks, R. E. Bruccoleri, B. D. Olafson, D. J. States, S. Swaminathan, M. Karplus, *J. Comp. Chem.* **1983**, *4*, 187 – 217.
[20] D. A. Pearlman, D. A. Case, J. W. Caldwell, W. R. Ross, T. E. Cheatham III, S. DeBolt, D. Ferguson, G. Seibel, P. Kollman, *Comp. Phys. Comm.* **1995**, *91*, 1 – 41.
[21] Q. Teng, Ph. D. Thesis, Florida State University, Tallahassee, FL, USA **1990**.
[22] M. Goldman, *Quantum Description of High Resolution NMR in Liquids*, Oxford, **1988**.
[23] K. Schmidt-Rohr, H. W. Spiess, *Multidimensional Solid-State NMR and Polymers,* Academic Press, **1994**.
[24] B. Mannfors, N. G. Mirkin, K. Palmo, S. Krimm, *J. Comput. Chem.* **2001**, *22*, 1933 – 1943.
[25] T. Head-Gordon, M. Head-Gordon, M. J. Frisch, C. K. Brooks, J. A. Popel, *J. Am. Chem. Soc.* **1991**, *113*, 5989 – 5997.
[26] R. Ditchfield, *Mol. Phys.* **1974**, *27*, 789 – 807.
[27] B. R. Brooks, R. E. Bruccoleri, B. D. Olafson, D. J. States, S. Swaminathan, M. Karplus, *J. Comp. Chem.* **1983**, *4*, 187 – 217, with the parameter set 22 forcefield, see: A. D. MacKerell, D. Bashford, M. Bellott, R. L. Dunbrack, Jr., J. D. Evanseck, M. J. Field, S. Fischer, J. Gao, H. Guo, S. Ha, D. Joseph-McCarthy, L. Kuchnir, K. Kuczera, F. T. K. Lau, C. Mattos, S. Michnick, T. Ngo, D. T. Nguyen, B. Prodhom, W. E. Reiher III, B. Roux, M. Schlenkrich, J. C. Smith, R. Stote, J. Straub, M. Watanabe, J. Wiórkiewicz-Kuczera, D. Yin, M. Karplus, *J. Phys. Chem.* **1998**, *102*, 3586 – 3616.
[28] M. Schaefer, M. Karplus, *J. Phys. Chem.* **1996**, *100*, 1578 – 1599.
[29] H. Susi, *Meth. Enzym.* **1972**, *26*, 455 – 472.

Received: January 2, 2007
Revised: April 12, 2007
Published online on May 25, 2007

